Astronomy & Astrophysics manuscript no. Lorentz
March 17, 2009

An implicit advection scheme for modeling relativistic shocks with high Lorentz factors

Hujeirat, A.A., Keil, B.W. and Hilscher, P.P.

ZAH, Landessternwarte Heidelberg-Königstuhl,
Universität Heidelberg, 69120 Heidelberg, Germany

Received ... / Accepted ...

ABSTRACT

Aims. A numerically stable and accurate advection scheme for modeling shock fronts moving at ultra-relativistic speeds is fundamentally important for understanding the thermodynamics of jets emanating from the vicinity of relativistic objects and the origin of the high gamma-rays.
Methods. In this paper we present a spatially third-order accurate advection scheme that is capable of capturing shock-fronts with diverse Lorentz factors. The consistency and accuracy of the scheme are investigated using the internal and total energy formulation in general relativity.
Results. Using the total energy formulation, the scheme is found to be viable for modeling moving shocks at moderate Lorentz factors, though with relatively small Courant numbers. In the limit of high Lorentz factors, the internal energy formulation in combination with a fine-tuned artificial viscosity is much more robust and efficient.
We confirm our conclusions by performing test calculations and compare the results with the analytical solutions of the relativistic shock tube problem.

Key words. Methods: numerical – hydrodynamics – relativistic – ultrarelativistic shocks

Received ... / Accepted ... General relativity: neutron stars – black holes – X-ray bursts, Methods: numerical – hydrodynamics – relativistic
Received ... / Accepted ...

1. Introduction

Plasmas moving at relativistic speeds have been observed in diverse astrophysical phenomena, such as in supernova explosions, in jets emanating from around neutron stars, microquasars and in active galactic nuclei (see Livio , 2004; Marscher , 2006; Fender et al. , 2007, and the references therein). The bulk Lorentz factor, Γ, of the observed jet-plasmas, in most cases, has been found to increase with the mass of the central relativistic object. Ejected plasmas from around neutron stars have $\Gamma_{NS} = O(1-3)$, in microquasars $\Gamma_{\mu QSO} = O(1-4)$ and in AGNs/QSOs $\Gamma_{AGN} = O(5-10)$. In gamma-ray bursts however, plasmas are considered to move with a Lorentz factor of the order of several hundreds (e.g., Piran, 2006), i.e., $\Gamma_{GRB} = O(100-1000)$.
Jet-plasmas considered to decelerate via self-interaction or interaction with the surrounding media in the form of shocks and eventually become efficient sources for the production of the observed high energy gamma-rays and probably for the energetic cosmic rays (Sikora, 1994).
Modeling the formation of relativistic shock by means of HD and MHD simulation has been the of focus of numerous studies during the the last two decades (Hawley et al., 1984b; Alay et al., 1999; Font et al., 2000; Marti and Müller, 2003; De Villiers, Hawley, 2003; Gammie et al., 2003; Anninos, Fragile, 2003; Komissarov, 2004; Del Zanna et al., 2007; Mignone et al., 2007; Hujeirat et al., 2008, see also the references therein).

These studies have enriched the field of computational astrophysics with numerical techniques and useful strategies for accurate capturing relativistic shock fronts using both the internal and total energy formulation (e.g., De Villiers, Hawley, 2003; Mignone et al., 2007). Nevertheless, most of the methods appear to encounter severe numerical difficulties whenever the Lorentz factor becomes large, i.e., $\Gamma \geq 5$. The reason is that small velocity errors are magnified by Γ^2 as they enter the other equations, hence inducing super-proportional errors in the estimation of the other variables. Recipes such as further reducing the grid spacing and accordingly the time step size my lead to stagnation of the solution procedure, particularly if the methods used are of time-explicit type.

The robustness of time-implicit methods at capturing shocks propagating with high Lorentz factors has been barely investigated, hence the purpose of the present paper. Moreover, we show that our time-implicit method in combination with a modified third order MUSCL advection scheme is capable of modeling shocks propagating with Lorentz factors $\Gamma \geq 10$ with time step sizes corresponding to Courant numbers larger than 1.

In Sec. 2 we describe the hydrodynamical equations solved in the present study. The solution method relies on using the 3D axi-symmetric general relativistic implicit radiative MHD solver (henceforth GR-I-RMHD), which has been described in details in a series of articles (e.g., Hujeirat et al., 2008; Hujeirat & Thielemann., 2009). In Sec. (3) we just focus on several new aspects of the advection scheme. The results of the verification tests is presented in Sec. (4) and end up with Sec. (5), where the results of the present study is summarized.

Send offprint requests to: A. Hujeirat, e-mail: AHujeirat@lsw.uni-heidelberg.de

2. The 1D general relativistic hydrodynamical equations

In the present study we consider the set of Euler equations in one-dimension and in flat spacetime:

$$\begin{aligned}&\partial_t \mathrm{D} + \nabla_\mathrm{r}\cdot(\mathrm{D}\,\mathrm{V}^\mathrm{r}) = 0\\ &\partial_t M_r + \nabla_r\cdot(M_r V^r) = -\partial_r P\\ &\partial_t \mathcal{E}^{\rm tot} + \nabla_r\cdot([\mathcal{E}^{\rm tot}+P]V^r) = 0,\end{aligned} \tag{1}$$

where $\nabla_\mathrm{r}\cdot = \frac{1}{\sqrt{-g}}\partial_\mathrm{r}\sqrt{-g}$, $\mathrm{D}(\doteq \rho \mathrm{u}^\mathrm{t})$ is the relativistic density, M_r is the radial momentum: $\mathrm{M}_\mathrm{r} \doteq \overline{\mathrm{D}}\mathrm{u}_\mathrm{t}$, where $\overline{\mathrm{D}} \doteq \mathrm{Dh}$, u^t is the time-like velocity[1] , $\mathrm{V}^\mathrm{r} = \mathrm{u}^\mu/\mathrm{u}^\mathrm{t}$ is the transport velocity, "h" is the relativistic enthalpy $\mathrm{h} = \mathrm{c}^2 + \varepsilon + \mathrm{P}/\rho$. $\mathcal{E}^{\rm tot} = (\mathrm{u}^\mathrm{t})^2\rho\mathrm{h} - \mathrm{P}$ is the total energy which is the sum of kinetic and thermal energies of the gas. "P" is the pressure of ideal gas: $\mathrm{P} = (\gamma-1)\rho\varepsilon$, ε and γ denote the internal energy and adiabatic index, respectively.

The reader is referred to Sec. (2) of Hujeirat et al. (2008), where the general relativistic hydrodynamical equations and their derivations in the Boyer-Lindquist coordinates are described. However, we continue to use these coordinates, though in the limit of flat space.
In the case that the mechanical energy is conserved, then the total energy reduces to an evolutionary equation for the internal energy:

$$\partial_\mathrm{t}\mathcal{E}^\mathrm{d} + \nabla_\mathrm{r}\cdot(\mathcal{E}^\mathrm{d}\mathrm{V}^\mathrm{r}) = -(\gamma-1)\,\frac{\mathcal{E}^\mathrm{d}}{\mathrm{u}^\mathrm{t}}[\partial_\mathrm{t}\mathrm{u}^\mathrm{t} + \nabla_\mathrm{r}\cdot(\mathrm{u}^\mathrm{t}\,\mathrm{V}^\mathrm{r})] \tag{2}$$

where $\mathcal{E}^\mathrm{d} = \mathrm{u}^\mathrm{t}\mathrm{P}/(\gamma-1)$.
Furthermore, there is a remarkable similarity of how Eq. (2) deals with $\mathcal{E}^\mathrm{d}$ and u^t. Taking this similarity into account, the equation can be re-formulated to have the following form:

$$\partial_\mathrm{t}\bar{\mathcal{E}}^\mathrm{d} + \nabla_\mathrm{r}\cdot(\bar{\mathcal{E}}^\mathrm{d}\mathrm{V}^\mathrm{r}) = -\gamma\mathrm{D}(\nabla_\mathrm{r}\cdot\mathrm{V}^\mathrm{r}), \tag{3}$$

where $\bar{\mathcal{E}}^\mathrm{d} = \mathrm{D}\log[\mathcal{E}^\mathrm{d}(\mathrm{u}^\mathrm{t})^{\gamma-1}]$.
In Equation (1), the energy equation describes the time-evolution of the total energy $\mathcal{E}^{\rm tot}$. Our numerical solution method relies first on selecting the primary variables and calculating their corresponding entries in the Jacobian. We then iterate to recover the correct contributions of the depending variables, such as the transport velocity and pressure. Therefore, the advection operator can be decomposed into two parts as follows:

$$\partial_\mathrm{t}\mathcal{E}^{\rm tot} + \nabla_\mathrm{r}\cdot(\mathcal{E}^{\rm tot}\mathrm{V}^\mathrm{i}) = \nabla_\mathrm{r}\cdot(\mathrm{P}\,\mathrm{V}^\mathrm{i}). \tag{4}$$

This equation is solved as follows: Solve for $\mathcal{E}^{\rm tot}$ using the pressure from the last iteration level. Once $\mathcal{E}^{\rm tot}$ and "D" are known, we may proceed to update the pressure as follows:

$$\mathrm{P} = \frac{\mathcal{E}^{\rm tot} - \mathrm{u}^\mathrm{t}\mathrm{D}}{\frac{\gamma}{\gamma-1}(\mathrm{u}^\mathrm{t})^2 - 1}. \tag{5}$$

This value of "P" is then inserted again into the RHS of Equation (4) to compute a corrected value for $\mathcal{E}^{\rm tot}$.
The effect of iteration can be reduced on the cost of using pressure values from the last time step using the following alternative formulation:

$$\partial_\mathrm{t}\tilde{\mathcal{E}}^{\rm tot} + \nabla_\mathrm{r}\cdot(\tilde{\mathcal{E}}^{\rm tot}\mathrm{V}^\mathrm{i}) = \partial_\mathrm{t}\mathrm{P}, \tag{6}$$

[1] u^t is also the general relativistic Lorentz factor, which reduces to Γ in flat space.

where $\tilde{\mathcal{E}}^{\rm tot} = (\mathrm{u}^\mathrm{t})^2\rho\mathrm{h}$.
Thus, once $\tilde{\mathcal{E}}^{\rm tot}$ is found, the pressure can be computed from the known conservative variables as follows:

$$\mathrm{P} = \frac{\gamma-1}{\gamma}\frac{\tilde{\mathcal{E}}^{\rm tot} - \mathrm{u}^\mathrm{t}\mathrm{D}}{(\mathrm{u}^\mathrm{t})^2}. \tag{7}$$

On the other hand, using the internal energy formulation for modeling moving shocks requires the inclusion of an artificial viscosity for calculating their fronts accurately. This modification is necessary in order to recover the loss of heat generally produced through the conversion of kinetic energy into internal energy at the shock fronts.
In this case, the RHS of Equation (2) should be modified to include the artificial heating term:

$$\mathrm{Q}^+_{\rm art} = \eta_{\rm art}(\partial_\mu \mathrm{u}^\mathrm{t}\mathrm{V}^\mu)^2, \tag{8}$$

where η_{art} is the artificial viscosity coefficient.
The inclusion of Q^+_{art} implies an enhancement of the effective pressure. Therefore, the thermodynamical pressure, and also the enthalpy, should be modified to include an artificial pressure of the form:

$$\mathrm{P}_{\rm tot} = \mathrm{P} + \mathrm{P}_{\rm art} = \mathrm{P} + \eta_{\rm art}\partial_\mu(\mathrm{u}^\mathrm{t}\mathrm{V}^\mu). \tag{9}$$

Note that the artificial pressure enters the momentum equation in the form of ∇P_{art}, which scales as $\sim \Delta(\eta_{art}V)$. This is equivalent to activating a second order viscous operator at the shock fronts, whose effect is then to transport information from the downstream to the upstream regions, so to enhance the stability of the transport scheme in such critical transitions.

2.1. Determining the Lorentz factor

Our test calculations showed that the Lorentz factor can be best determined from the normalization condition, in which both the conservative variables and transport velocities are involved. To clarify this point, the normalization condition reads:

$$\begin{aligned}-1 &= u^\mu u_\mu\\ &= (u^t V^\mu)\,(\tfrac{M_\mu}{D})\\ &= \tfrac{u^t}{D}[M_t + V^r M_r + V^\theta M_\theta + V^\varphi M_\varphi]\\ &= \tfrac{u^t}{D}[\{\tfrac{M^t - g^{t\varphi}M_\varphi}{g^{tt}}\} + V^\theta M_\theta + V^\varphi M_\varphi]\\ &= \tfrac{u^t}{D}[(\tfrac{\bar{D}u^t}{g^{tt}}) + V^\theta M_\theta + (V^\varphi - \tfrac{g^{t\varphi}}{g^{tt}})M_\varphi],\end{aligned} \tag{10}$$

where $\bar{\mathrm{D}} = \rho\mathrm{h}\mathrm{u}^\mathrm{t}$ and which can be directly determined from the continuity and the energy equations, V^μ is the transport velocity and $\mathrm{g}^{\mu\nu}$ are the elements of the metric.
The final form of Eq. (10) is the quadratic equation: $\mathrm{a}\,(\mathrm{u}^\mathrm{t})^2 + \mathrm{b}\,\mathrm{u}^\mathrm{t} + \mathrm{c} = 0$, from which the Lorentz factor can be determined completely.
We note that since the state of the conservative variables D, $\mathrm{M}_\mu, \mathcal{E}^\mathrm{d}$ depends strongly on the transport velocity V^μ, it is therefore necessary to consider V^μ when computing the Lorentz factor u^t as described in Eq. (10).

3. A modified third order advection scheme for high Lorentz factors

Most time-implicit advection schemes generally rely on upwinding to stabilize the transport near critical fronts. Transport of quantities here can be mediated with CFL numbers larger than unity. Therefore, the advection scheme employed should be independent of the time step size. Indeed, the monotone upstream

centered schemes for conservation laws, or simply the MUSCL schemes, obey these conditions (see Hirsch, 1988, and the references therein). However, in order to model moving shocks with high Lorentz factors accurately, it is necessary to modify the scheme, so that the information-flow from the downstream to upstream regions should be further limited in accordance with the normalization condition, i.e., causality condition.
A classical advection scheme of the MUSCL-type gives the following interface values:

$$\begin{array}{ll} q^{SR}_{j-1/2} = q_{j-1} - \frac{1}{4}[(1+\kappa)\Delta q_{j-1} + (1-\kappa)\Delta q_{j-2}] & : \text{if} \quad V_j \le 0 \\ q^{SL}_{j-1/2} = q_j \ + \ \frac{1}{4}[(1-\kappa)\Delta q_j + (1+\kappa)\Delta q_{j+1}] & : \text{if} \quad V_j > 0, \end{array} \tag{11}$$

where "q" is the transported physical quantity, κ is a switch off/on parameter that specify the accuracy needed and $\Delta q_j = q_j - q_{j+1}$. Note that the scheme is of second order for $\kappa = -1, 0, 1$ and of third order for $\kappa = 1/3$.
In order to enable an accurate capturing of shock fronts propagating with high Lorentz factors on a non-uniform grid distribution, the following modifications have been performed:

$$\begin{array}{l} \text{if} \quad V_j \le 0: \quad q^{SR}_j = q_{j-1} - \frac{1}{4}[(1-\sigma)\Delta q_j + (1+\sigma)\Delta q_{j-1}], \\ \quad \text{where} \quad \sigma = 2\kappa\,(\Delta q^{RR}_j \cdot \Delta q^{0R}_j)/[(\Delta q^{RR}_j)^2 + (\Delta q^{0R}_j)^2 + \epsilon]. \\ \text{if} \quad V_j > 0: \quad q^{SL}_j = q_j + \frac{1}{4}[(1+\sigma)\Delta q_j + (1-\sigma)\Delta q_{j+1}], \\ \quad \text{where} \quad \sigma = 2\kappa\,(\Delta q^{0L}_j \cdot \Delta q^{LL}_j)/[(\Delta q^{0L}_j)^2 + (\Delta q^{LL}_j)^2 + \epsilon], \end{array} \tag{12}$$

where

$$\begin{array}{l} \Delta q^{RR}_j = (x^m_{j-1} - x^m_j)(q_{j-2} - q_{j-1})/(x^m_{j-2} - x^m_{j-1}) \\ \Delta q^{0R}_j = (x^m_{j-2} - x^m_{j-1})(q_{j-1} - q_j)/(x^m_{j-1} - x^m_j) \\ \Delta q^{0L}_j = (x^m_j - x^m_{j+1})(q_{j-1} - q_j)/(x^m_{j-1} - x^m_j) \\ \Delta q^{LL}_j = (x^m_{j-1} - x^m_j)(q_j - q_{j+1})/(x^m_j - x^m_{j+1}), \end{array} \tag{13}$$

and where ϵ is a small number set to avoid division by zero.

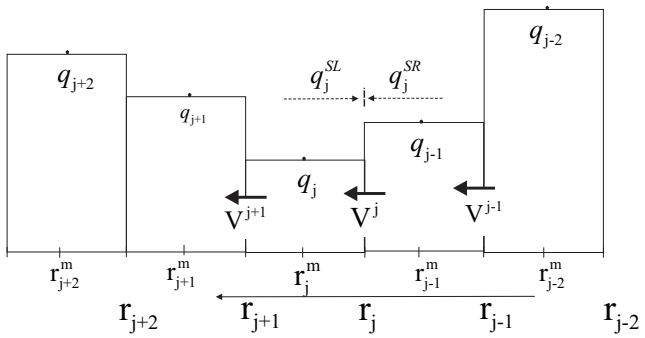

Fig. 1. A schematic description of several finite volume cells, their boundaries and the location of the scalar quantities "q" and the velocities.

The accuracy of above modified scheme may be further increased by incorporating the Lagrangian Upwind Interpolation Scheme (LUIS). The LUIS strategy is based on by constructing a Lagrangian polynomial of third or fourth order whose main weight is shifted to the right or left, depending on the upwind direction. The final combined LUIS-MUSCL scheme reads as follows:

$$\begin{array}{ll} \text{if} \quad V_j \le 0: & q^{SR}_j = \xi q^{SR}_j + (1-\xi) Lq^{SR}_j, \\ \text{if} \quad V_j > 0: & q^{SL}_j = \xi q^{SL}_j + (1-\xi) Lq^{SL}_j, \end{array} \tag{14}$$

where ξ is an additional weighting function and $Lq^{SR,SL}_j$ are LUIS corrections of "q" at the interface r_j (see Fig. 2, which are computed in the following manner:

$$\begin{array}{ll} Lq^{SR}_j = \sum_{l=j-2}^{l=j} q_l \prod_{i\neq k, k=j-2}^{k=j} \frac{r_j - r^m_k}{r^m_i - r^m_k}, & : \text{if} \quad V_j \le 0 \\ Lq^{SL}_j = \sum_{l=j}^{l=j+2} q_l \prod_{i\neq k, k=j}^{k=j+2} \frac{r_j - r^m_k}{r^m_i - r^m_k}, & : \text{if} \quad V_j > 0. \end{array} \tag{15}$$

However, we note that high order advection schemes generally degenerate into lower ones at the shock fronts or discontinuities, in order to maintain monotonicity of the advection scheme, which in turn enhances the production of numerical entropy/diffusion at these critical transitions. Therefore, in most of the test calculations presented here it was necessary to have $\xi > 1/2$, or even very close to unity to enable convergence.

4. Results

In this section we present results of various verification tests using different energy formulations in combination with the advection scheme described in the previous section. The widely used hydrodynamical test is the one-dimensional relativistic shock tube problem (henceforth RSTP). The advantages of this test problem is that the obtained numerical solutions can be compared with the corresponding analytical solution with arbitrary large Lorentz factors.
For further details on the background of this test problem and the way the analytical solutions are obtained we refer the reader to (Marti and Müller, 2003).
The RSTP is an initial value problem, in which the solution depends strongly on the initial conditions. So the domain of calculations is divided into a right and left regions (see Fig. 2). In the left region $0 \le x \le x_c$: we set $P_L = 40/3$, $\rho_L = 10$ and in the right region $x_c < x$: we set $P_R = (2/3) \times 10^{-6}$, $\rho_R = 1$. The initial velocity is set to vanish everywhere.

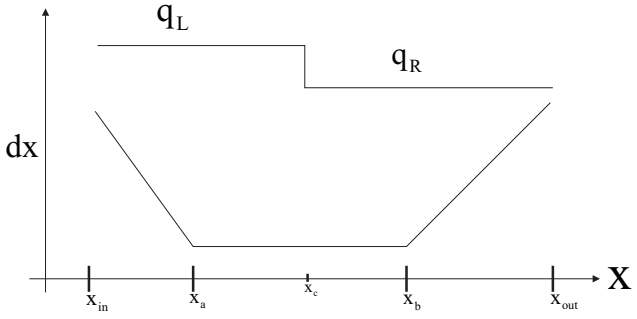

Fig. 2. Grid spacing versus position. The actual changes of the variables occur in the interval $[x_a \le x \le x_b$, where the grid spacing is uniform. The initial conditions read: for $x \le x_c$: $P_L = 40/3$, $\rho_L = 10$ and for $x > x_c$: $P_R = (2/3) \times 10^{-6}$ and $\rho_R = 1$.

Using the total energy formulation (TEF) we show in Figures (3-13) the profiles of the velocity and the corresponding Lorentz factor for different distributions of the initial conditions.
In Fig.3 we show the profiles of the velocity and Lorentz factor after 0.2 sec using the total energy formulation (see Eq. 1). The interval $[0.35 \le x \le 0.75]$ has be divided into 400 equally spaced cells, whereas 220 cells where used to cover the external intervals, where the variables continue to acquire their initial values. The advection scheme described in (Eq. 14) has been employed to achieve 3rd order spatial accuracy and the damped

Crank-Nicolson method is used to achieve second order temporal accuracy (Hujeirat, Rannacher, 2001). The time step size is set to have a maximum that corresponds to CFL= 0.4.

To test the robustness of the solution procedure, we have increased the P_L by a factor of 100, while the other variables remained unchanged. This increase of the pressure yields the Lorentz factor: $u^t \approx 3.6$ (Fig. 4). However, to enforce convergence, it was necessary to increase the number of iteration per time step considerably.

Comparing the results with those of Fig. (5), we see that the solution obtained is sufficiently accurate, so that doubling the number of grid points and decreasing the time step size by half did not improve the accuracy of the scheme significantly.

From Figs. (6) and (7), we see that incorporating artificial viscosity and artificial heating while using the TEF has a similar effect as that of the normal numerical diffusion. In both cases the velocity at the shock front attains lower values than expected from the analytical solution.

We note that within the context of time-implicit solution methods, the total energy method appear to have a limited capability to capture shocks moving with high Lorentz factors (Fig. 8). The reason is that, unlike the internal energy E_{in}, the kinetic energy E_{kin} increases with Lorentz factor as Γ^2. As a consequence, the convergence rate decreases with E_{in}/E_{kin}. In this case it is necessary to decrease both the time step size and the grid spacing in addition to increasing the number of iteration per time step. This procedure may easily lead to a stagnation of the solution method.

On the other hand, our time-implicit solution method appears to be more robust if the internal energy formulation is used. In Figures (9-13), the results of several test calculations are shown, which agree well with the analytical solutions. Moreover, the IEF is sufficiently stable, so that running the calculations with CFL ≥ 1 does not appear to hinder the convergence of the implicit solution procedure (see Figs. 12 and 13).

The major draw back of the IEF is the necessity to fine-tune the coefficients of the artificial viscosity in order to obtain the correct Lorentz factor that fits well with the analytical solution. Moreover, these fine-tuning procedures of the parameters must be repeated each time the ratio of the pressure P_L/P_R is changed. This is a consequence of the conversion of kinetic energy into heat at the shock fronts which cannot be determined a priori and uniquely by solving the internal energy alone.

Nevertheless, using the IEF, non-linear physical processes can be easily incorporated into the implicit solution procedure. Unlike in the TEF case, such processes are direct functions of the internal energy and therefore it is much easier to compute their entries and incorporate them into the corresponding Jacobian. This has the consequence that calculations can be performed also with CFL ≥ 1, while still maintaining consistency with the original physical problem.

Finally, in Fig. (14) we show the profiles of V and u^t using the compact internal energy formulation (CIEF, Eq.(3) with high accuracies. The method is found to display overshooting and undershooting both at the contact discontinuity and the shock front, whose appearing was difficult to prevent through enlarging the number of grid points, decreasing the time step, enhancing the number of iteration per time step or even by activating the artificial viscosity.

It should be noted here that since in the limit of large Lorentz factors, the CFL number depends weakly on the sound speed (see Fig. 15), increasing the global iteration per time step has more significant effect on convergence than merely decreasing the time step size.

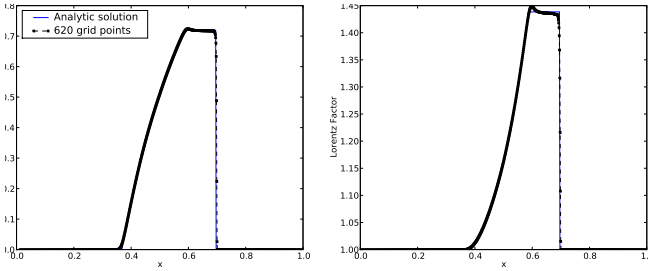

Fig. 3. The profiles of the velocity V (left) and the Lorentz factor u^t (right, dashed line connecting squares) overplotted on the corresponding analytical solutions (continuous blue lines) after $\tau = 0.2$. The numerical solutions have been obtained using the total energy formulation (TEF), the initial pressure ($P_{L0} = 40/3$, $\rho_L = 10$), ($P_R = (2/3) \times 10^{-6}$, $\rho_R = 1$), 700 non-uniformly distributed grid points and CFL=0.4. The advection scheme employed here is of third order spatial and second order temporal accuracy.

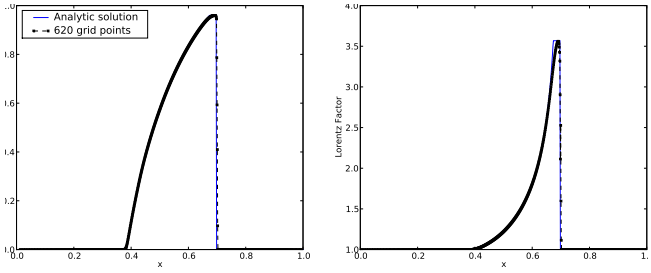

Fig. 4. As in Fig (3), the profiles of V and u^t have been obtained using the TEF, an initial pressure $P_L = 10^2 P_{L0}$ and CFL= 0.4. 620 non-uniformly distributed grid points have been used

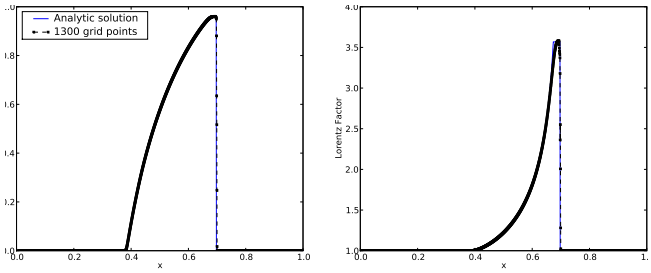

Fig. 5. As in Fig (3), the profiles of V and u^t have been obtained using the TEF, an initial pressure $P_L = 10^2 P_{L0}$, CFL= 0.4 and 1300 non-uniformly distributed grid points.

5. Summary and conclusions

In this paper we have presented the results of different numerical studies for modeling the propagation of ultra-relativistic shocks using the internal energy (IEF), the total energy (TEF) and pseudo-total energy (PTEF) formulations.

Our test calculations show that TEF is most suited for modeling the propagation of shocks with low to moderate Lorentz factors, though with low CFL numbers, hence more suitable for time-explicit solution methods.

On the other hand, although the PTEF is similar to the TEF, it was found that a larger number of iterations per time step was required to maintain convergence.

Using the IEF however, it was verified that the implicit solution procedure converges relatively fast even for a Lorentz factor $u^t \gg 1$ and a CFL number of CFL ≥ 1.

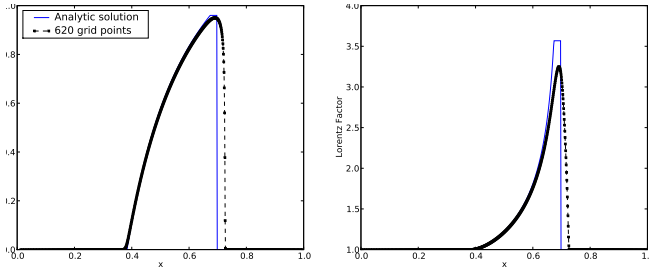

Fig. 6. As in Fig (3), the profiles of V and u^t have been obtained using the TEF, an initial pressure $P_L = 10^2 P_{L0}$, a CFL= 0.4. An upwind advection scheme of first order spatial accuracy has been used.

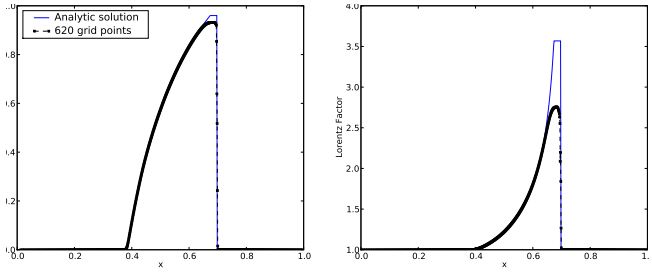

Fig. 7. As in Fig (3), the profiles of V and u^t have been obtained using the TEF with a heating source due to artificial viscosity, an initial pressure $P_L = 10^2 P_{L0}$, CFL= 0.4 and a spatially third order accurate advection scheme.

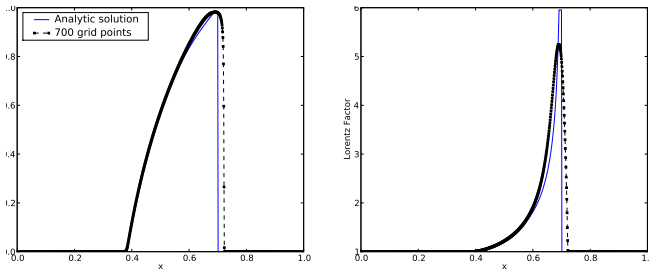

Fig. 8. As in Fig (3), the profiles of V and u^t have been obtained using the pseudo-total energy formulation (PTEF, see Eq. 6), an initial pressure $P_L = 10^3 P_{L0}$ and CFL= 0.4.

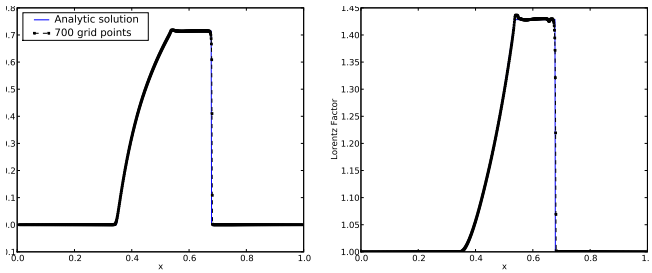

Fig. 9. As in Fig (3): the profiles of V and u^t have been obtained using the internal energy formulation (IEF, see Eq. 2), an initial pressure $P_L = P_{L0}$ and CFL= 0.4.

It should be stressed here that the IEF has a major draw back, as it requires a fine-tuned parameters of the artificial viscosity to obtain the correct Lorentz factor at the shock fronts. On the other hand, when modeling astrophysical plasmas, the IEF is favorable over the TEF, as cooling and heating processes are in general direct functions of the internal energy, thus it is easier to construct the corresponding coefficients and incorporate them into the Jacobian.

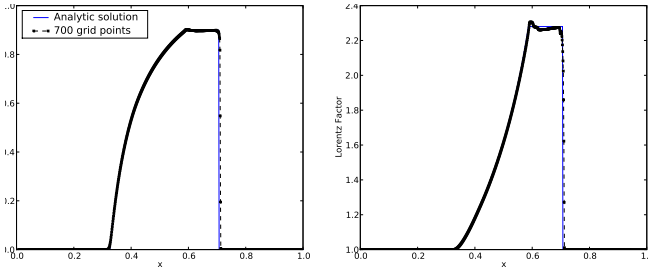

Fig. 10. Similar to Fig (3), the profiles of V and u^t have been obtained using the IEF with the initial left pressure $P_L = 10 P_{L0}$. The rest of variables remained as in Fig. (1) unchanged.

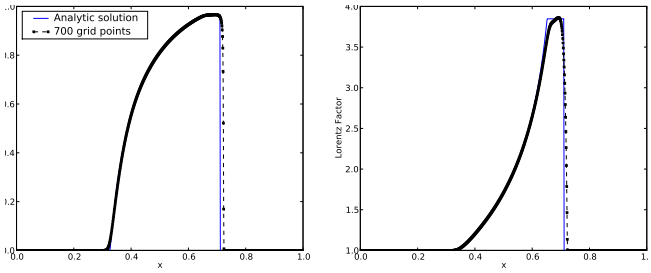

Fig. 11. As in Fig (3), the profiles of V and u^t have been obtained using the IEF, an initial pressure $P_L = 10^2 P_{L0}$ and a CFL = 1.5 after $\tau = 0.215$.

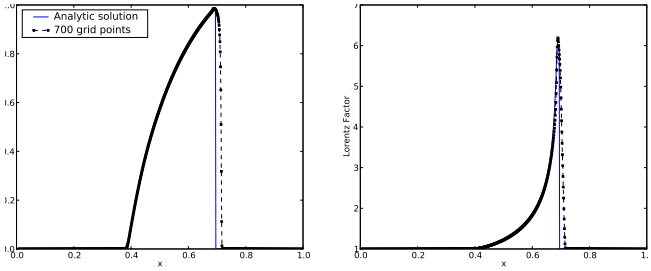

Fig. 12. As in Fig (3), the profiles of V and u^t have been obtained using the IEF, an initial pressure $P_L = 10^3 P_{L0}$ and a CFL= 2.

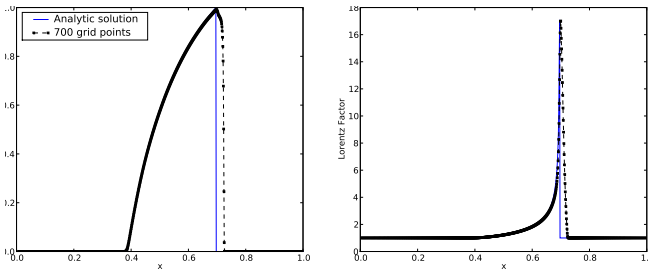

Fig. 13. As in Fig (3), the profiles of V and u^t have been obtained using the IEF, an initial pressure $P_L = 10^5 P_{L0}$ and a CFL= 4.

Furthermore, turbulence is an important property of most astrophysical fluid flows. Thus the artificial viscosity in such flows naturally will be overwhelmed by turbulent diffusion, hence relaxing the fine-tuning problem of the artificial viscosity.

Irrespective of the method used for solving the energy equation, the Lorentz factor is found to be best computed from the normalization condition in which the transport velocities and

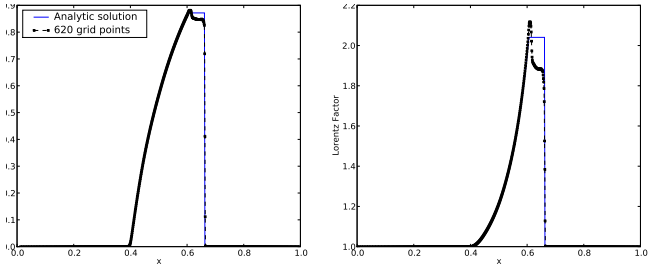

Fig. 14. As in Fig (3), the profiles of V and u^t after $\tau = 0.175$ have been obtained using the compact internal energy formulation (CIEF, see Eq. 3) and the initial pressure $P_L = 10P_{L0}$.

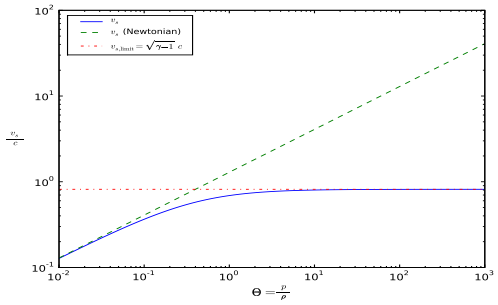

Fig. 15. $\beta = V_S/c$ for the Newtonian case ($V_S = \gamma P/\rho$; dashed line) and for the relativistic case ($V_S = \gamma P/\rho h$; solid line) versus temperature.

momenta are used.

We have also presented a modified MUSCL advection scheme of third order spatial accuracy, which has been constructed to enable accurate capturing of relativistically moving shocks. The accuracy of the scheme can be further enhanced by incorporating the Lagrangian Upwind Interpolation Scheme (LUIS).
On the other hand, using this advection scheme for modeling astrophysical fluid flows may unnecessary increase the computational costs, in particular when 3D axi-symmetric calculations with high resolution are required.

Noting that the appropriate parameters of the artificial viscosity cannot be determined a priori, obtaining the correct Lorentz factor may turn out to be a difficult task. In the case of standing shocks, the hierarchical solution scenario (Hujeirat, 2005) can be employed to gradual enhance the accuracies of the scheme to obtain the correct Lorentz factors at the shock fronts.
In a forthcoming paper, we intend to study the formation of strong shocks in curved spacetime near the surface of ultra-compact neutron stars.

Acknowledgment This work is supported by the Klaus-Tschira Stiftung under the project number 00.099.2006.

References

Biretta, J.A., 1999, AAS, 195, 5401
Marscher, A.P., 2006, AIPC, 856, 1
Aloy, M.-A., Ibanez, J.M., Mart, J.M., Müller, E., 1999, ApJS, 122, 151 (GENESIS)
Anninos, P., Fragile, P. C., 2003, ApJ. Suppl. Ser., 144, Iss. 2, 243-257
Del Zanna, L., Bucciantini, N., 2002, A&A, 390, 1177-1186
Del Zanna, L., Zanotti, O., et al., 2007, A&A, 473, 11
De Villiers, J.-P., Hawley, J.F., 2003, ApJ, 589, 458
Fender, R., Koerding, E., Belloni, T., et al. 2007, astro-ph, 0706.3838
Font, J.A., Miller, M., Suen, W., Tobias, M., 2000, Phys. Rev. D, 61, 044011
Font, J.A., 2003, LRR, 6, 4
Gammie, C. F., McKinney, J. C., Tóth, G., 2003, ApJ, 589, 444-457 (HARM)
Hirsch, C., 1988, "Numerical Computation of Internal and External Flows", Vol. I, II, John Wiley & Sons, New York
Hujeirat, A., Rannacher, R., 2001, New Ast. Reviews, 45, 425
Hujeirat, A., 2005, CoPhC, 168, 1
Hujeirat, A., Camenzind, M., Keil, B.W., 2008, New Astronomy, 13, 436
Hujeirat, A., Thielemann, F.-K., 2009, A&A, to appear
Hawley, J. F., Smarr, L. L., Wilson, J. R., 1984a, ApJ, 277, 296-311
Hawley, J. F., Smarr, L. L., Wilson, J. R., 1984b, ApJS, 55, 211-246
Koide, S., Shibata K., Kudoh, T., 1999, ApJ, 522, 727
Komissarov, S.S., 2004, MNRAS, 350, 1431
Livio, 2004, BaltA, 13, 273L
Marti, J.M., Müller, E., 2003, LRR, 6, 7
Mignone, A., Bodo, G., Massaglia, et al., 2007, ApJS, 170, 228-242 (PLUTO)
Mizuno, Y., Nishikawa, J.-I., et al., 2006, astro-ph/0609004 (RAISHIN)
Piran, T., 2005, RvMP, 76, 1143
Sikora, M., Begelman, M.C., Rees, M.J., 1994, ApJ, 421, 153